JOURNAL OF MATERIALS SCIENCE

# A comparative analysis of copper and brass surface films in contact with tap water

M. B. VALCARCE, S. R. DE SÁNCHEZ, M. VÁZQUEZ*
*División Corrosión, INTEMA, Facultad de Ingeniería, UNMdP, Juan B. Justo 4302, B7608FDQ Mar del Plata, Argentina*
*E-mail: mvazquez@fi.mdp.edu.ar*

**Published online:** xx2 xx

A study of the surface oxide films naturally grown on copper and brass in contact with drinkable water is presented. The investigation focuses on the influence of Zn as alloying element on the corrosion resistance of brass. Artificial tap water, employed as electrolyte, simulates a practical application of these materials. The surface films were grown at open circuit potential for 2 and 192 hours. Diverse *in-situ* techniques such as cyclic voltammetry, polarization curves, electrochemical impedance spectroscopy and UV-Vis reflectance spectroscopy were employed. Even when the surface layer is mainly composed of cuprous oxide, Zn(II) species are incorporated in the surface film grown on brass. At longer ageing times, the thickness increases, without affecting the composition of the surface films. The corrosion current was calculated for both materials using various techniques. The corrosion current density and the anodic currents in the polarization curves decreased as the ageing time increased, particularly in the case of brass. This improvement in the performance of the film on brass can be attributed to the incorporation of Zn(II) species into the surface layer, particularly as the film consolidates at longer times.




## 1. Introduction

Copper and copper alloys such as brasses are frequently used in tap-water distribution systems [1–5]. A protective oxide layer grows naturally on their surface, which prevents further corrosion from the base metal. The corrosion resistance of the various alloys strongly depends on the performance of their protective passive film. On copper-based substrates, the film is primarily composed of $Cu_2O$. To improve their performance against corrosion in aggressive environments, the global composition can be modified by the incorporation of alloying elements.

The piping system of many potable water installations has frequently found to be affected by pitting. In many of these cases, microbiologically influenced corrosion has proven to be the origin of the problem [6–8]. The stability of the passive film and its ability to prevent damage depend on film composition and thickness. The work presented in this paper is part of an on-going investigation on the effect of *Pseudomonas fluorescens* on the corrosion of copper alloys in contact with tap water [9–11].

Many investigations published in leading journals over the last years have addressed the various issues that govern copper corrosion in drinking waters [1–4, 12, 13]. Others have studied the effect of diverse alloying elements and different electrolytes on the corrosion processes of brasses [14–17]. This study focuses on the influence of Zn as alloying element on the improvement of the corrosion resistance of Al-brass (Cu75Zn23Al2), using artificial tap water (ATW, pH = 7.6) as electrolyte. Other variables that also participate in the process, such as the presence of microorganisms and bacterial adhesion in this same system, have been described elsewhere [9–11].

Film properties such as composition and thickness are evaluated by a combination of electrochemical and spectroelectrochemical techniques. Copper, zinc and Al-brass are compared so as to investigate the influence of Zn as alloying element.

## 2. Experimental

### 2.1. Electrodes preparation

Disc samples of copper, zinc and aluminum brass (Cu 75%, Zn 22.18% and Al 1.8%, UNS 68700) were included in fast curing acrylic resin on appropriated PVC holders. An electrical contact was prepared at the back of each sample. The electrodes were polished down to grade 600 with emery paper, and finally mirror polished with 0.05 $\mu$m alumina powder (Type B−Buehler, Lake Bluff, USA). The electrodes were then rinsed gently with distilled water.

*Author to whom all correspondence should be addressed.
0022-2461 
DOI: 10.1007/s10853-005-4499-6

## 2.2. Electrolyte composition

Most of the experiments were carried out using artificial tap water (ATW). The mineral base composition was $MgSO_4$ (40 mg $l^{-1}$), $MgCl_2$ (60 mg $l^{-1}$), $KNO_3$ (25 mg $l^{-1}$), $CaCl_2$ (110 mg $l^{-1}$), $Na_2CO_3$ (560 mg $l^{-1}$) and $NaNO_3$ (20 mg $l^{-1}$) in distilled water; the pH was adjusted to 7.6 with HCl 1 molar solution.

Boric-borate buffer (pH = 7.8) was used as electrolyte where indicated, in order to compare the results with those well-established by other authors [18–21].

All the experiments were carried out at room temperature (20 ± 2°C).

## 2.3. Electrochemical techniques

A three-electrode electrochemical cell was used. A saturated calomel electrode (SCE, E = 0.24 V vs. NHE) was used as reference. All the potentials are indicated against SCE. A platinum wire of large area was used as counter electrode.

The electrochemical instrumentation included a Voltalab PGP 201 potentiostat and a Solartron SI 1280B unit.

Cyclic voltammograms were recorded after deaerating the electrolyte, bubbling $N_2$ during 15 min prior to each measurement. The electrodes were pre reduced in ATW at −1.1 V for five minutes. Finally the scan was started at –1.1 V and reversed at convenient potential values. The sweep rate was 0.01 V $s^{-1}$.

Film growth was investigated carrying out potentiodynamic reductions. The electrodes were prereduced in ATW at –1.1 V for 15 min to obtain a reproducible, clean surface. After that, the passive film was grown on the metallic surfaces at open circuit potential (OCP) during two different times: 2 and 192 h. Then the electrodes were immediately transferred to another cell where the oxides were reduced in deareated electrolyte applying a potentiodynamic scan at $10^{-4}$ V $s^{-1}$. The potential was scanned in the negative direction, starting at OCP and up to –1.1 V.

Polarization resistance ($Rp$) was evaluated as $\Delta V/\Delta i$, from potential sweeps scanning ± 0.01 V from $E_{corr}$ at a scan rate of $10^{-4}$ V $s^{-1}$. The electrodes were previously aged for 2 and 192 h at OCP. Corrosion rate, in terms of corrosion current density, can be evaluated from the polarization resistance data according to the Stern-Geary relationship [22] as:

$$i_{corr} = \frac{\beta_a \beta_c}{2.303\,(\beta_a + \beta_c)} \frac{1}{Rp} = \frac{B}{Rp} \qquad (1)$$

where $\beta_a$ and $\beta_c$ are the anodic and cathodic Tafel slopes respectively. These are kinetic parameters characteristic of each metal-solution system.

The corrosion current density can also be evaluated from the intersection of the polarization curves at the corrosion potential. The curves were recorded after holding the electrodes 2 and 192 h at OCP. Anodic and cathodic polarization curves started at OCP and were recorded at $10^{-4}$ V $s^{-1}$ in independent experiments.

## 2.4. Electrochemical impedance spectroscopy

Electrochemical impedance spectroscopy (EIS) tests were performed at open circuit potential (OCP). Recording each spectrum took between 90 and 160 min. Prior to starting the frequency sweep, the samples were pretreated for 15 min at −1.1 V and then kept for 2 or 192 h in contact with ATW. The solution was used without stirring or deareation. The amplitude of the AC voltage signal was ± 0.01 V while the frequency varied between 20 kHz and 1 mHz. The results were analyzed using the equivalent circuit presented in Fig. 1. This circuit is typical of oxide-coated metals and has been used before by other authors in relation to copper corrosion in potable water [1, 2]. The experimental data were fitted to the proposed equivalent circuit using ZView™ [23]. Corroding electrodes can show various types of inhomogeneities, which can be represented by the inclusion of constant phase elements (CPE) in place of capacitors in the equivalent circuit. Surface roughness, insufficient polishing, grain boundaries and surface impurities had been mentioned before among the main reasons allowing the use of CPEs in equivalent circuits of corroding electrodes [24]. The impedance of this element is frequency-dependent, and can be mathematically expressed using two parameters, Q and $n$ as:

$$Z_{CPE} = [Q(j\omega)^n]^{-1} \qquad (2)$$

where $Q$ is a constant with dimensions of Ω $cm^2$ $s^{-(1-n)}$ and $n$ a constant power, with $-1 < n < 1$. According to the value of $n$, Equation 2 accounts for an inductance ($n = -1$), a resistance ($n = 0$), a Warburg impedance ($n = 0.5$) or a capacitance ($n = 1$). A Warburg element occurs when charge carriers diffuse through a material. A rough or porous surface can cause a double layer capacitance to appear as a constant phase element with $n$ varying between 0.5 and 1.

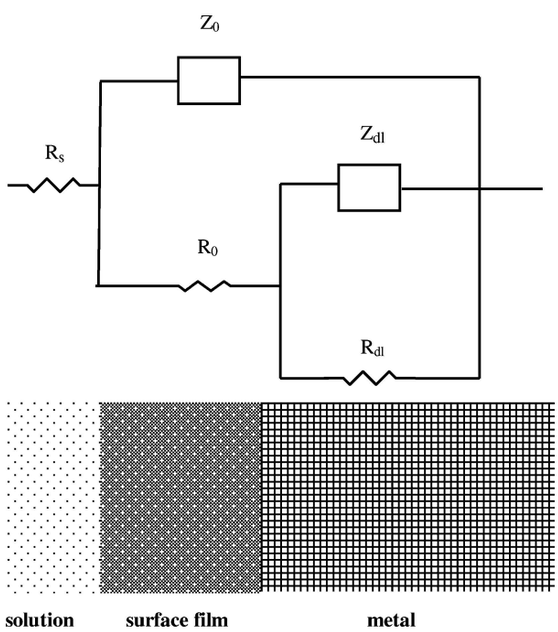


*Figure 1* Equivalent circuit proposed for interpreting the EIS response.

### 2.5. UV-visible reflectance spectroscopy

The film growth was also evaluated using reflectance spectroscopy. The corresponding absorption spectra were recorded *in-situ*. Baseline corrections were carried out by polarizing two identical polished surfaces at –1.1 V during 15 min to prevent oxide growth. Surface oxides were grown holding aluminum brass, zinc and copper at OCP for 30, 60, 90 and 120 min. Ageing was performed in the samples compartment. The spectrum of each material was recorded in aerated electrolyte.

The spectroelectrochemical measurements were carried out using a commercial double-beam spectrophotometer (Shimadzu UV 160A), conveniently modified as described elsewhere [25, 26].

## 3. Results

### 3.1. Characterization of copper and brass surfaces by cyclic voltammetry

Fig. 2 shows the cyclic voltammogram of copper in deaerated artificial tap water (ATW) and in borax buffer pH 7.8.

In the case of ATW, oxide growth starts at potentials positive to –0.33 V. A sharp anodic peak (Ia) is evident at –0.2 V and localized corrosion initiates at potentials positive to 0.05 V. Three cathodic peaks appear at −0.11 (Ic), –0.49 (IIc) and –0.9 V (IIIc). Cathodic peak Ic can be assigned to the reduction of Cu(II) species while peak IIc can be attributed to the reduction of Cu(I) species. A third cathodic peak (IIIc) next to the beginning of the hydrogen evolution region has been found before [10, 27, 28] and it has been associated to the reduction of soluble Cu(I) species. The anodic sweep was reverted at various different potentials so as to correlate anodic and cathodic peaks. When the scan is reverted at –0.1 V the cathodic peak Ic is no longer present, while the intensity of peaks IIc and IIIc decreases. If the scan direction is inverted at –0.3 V, only peak IIIc remains as a shoulder in the voltammogram. No cathodic peak can be seen only when the scan is reversed at –0.6 V.

In contrast, in the borax solution the anodic peak is located at 0 V. A small anodic current at –0.45 V has been attributed to the formation of a CuOH monolayer adsorbed on the surface [16, 27, 29]. In the cathodic region two peaks can be observed: Ic' at −0.11 V and IIc' at –0.44 V. These have been attributed to the reduction of Cu(II) and Cu(I) compounds respectively.

The voltammograms of pure Zn in ATW and borax solution are presented in Fig. 3. In ATW, oxide growth starts at potentials positive to −1.3 V. Peak Ia appears at −1.15 V and the electrode presents localized corrosion at potentials positive to −0.81 V. The corresponding cathodic peak (Ic) can be seen at −1.4 V.

The voltammograms of Zn in the borax buffer solution shows an anodic peak (Ia′) at −0.86 V that can be attributed to ZnO formation, while the corresponding reduction peak (Ic′) appears at −1.3 V [16, 28, 29]. The peak related to the Zn/ZnO equilibrium should appear at −1.09 V vs. SCE at pH = 7.6. The positions of the peaks in Fig. 3 are in agreement with the predicted value. ZnO can dissolve to form zincates only at pH values higher than 10 [30]. In the case of brass (Fig. 4), the cyclic voltammogram in ATW shows an anodic peak IIa at –0.80 V and a shoulder (Ia) for potentials higher than –0.25 V. Localized corrosion initiates at 0.05 V. The cathodic peak Ic at –0.3 V can be attributed to the reduction of cuprous compounds, while peak IIc at –0.99 V appears to be related to the reduction of Zn(II) species [10]. The potential where the scan is reverted was progressively moved in the negative direction. If the limit is between –0.2 and –0.8 V only peak IIc remains in the voltammogram.

When the cyclic voltammogram of brass is carried out in the borax solution, two anodic peaks can be seen at –0.04 and –0.7 V, labeled Ia' and IIa' respectively. The three cathodic peaks are located at –0.2, –0.38 and –0.84 V and labeled Ic', IIc' and IIIc', respectively. The first one has been attributed to Cu(II) compounds, the second to the reduction of Cu(I) species while the third one corresponds to Zn(II) reduction [28, 29].

### 3.2. Characterization of the surface films formed at open circuit potential by reflectance spectroscopy and potentiodynamic reduction curves

In ATW, both copper and brass reach the steady-state open circuit potential (OCP) after 2 h of immersion.

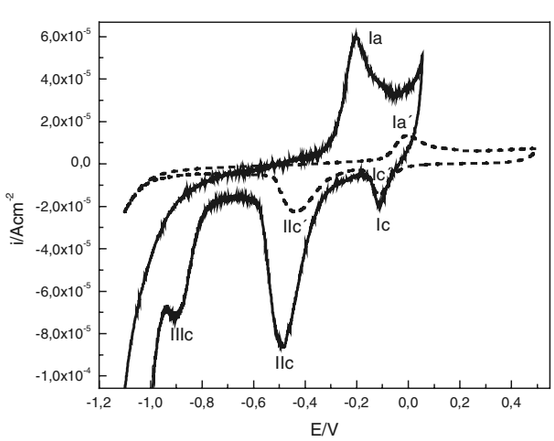


*Figure 2* Cyclic voltammogram of copper in deaerated artificial tap water (ATW) (—) and in borax buffer pH 7.8 (- - -). Scan rate: 10 mV $s^{-1}$.

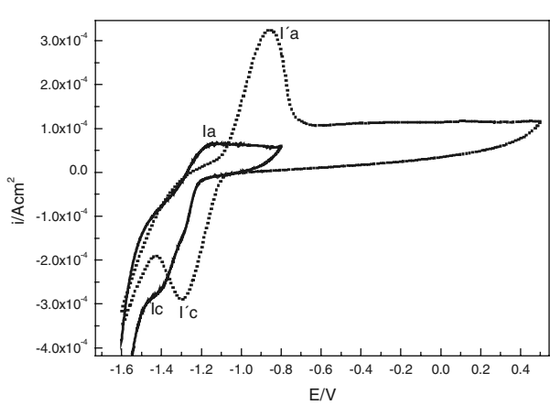


*Figure 3* Cyclic voltammogram of zinc in deaerated artificial tap water (ATW) (—) and in borax buffer pH 7.8 (- - -). Scan rate: 10 mV $s^{-1}$.

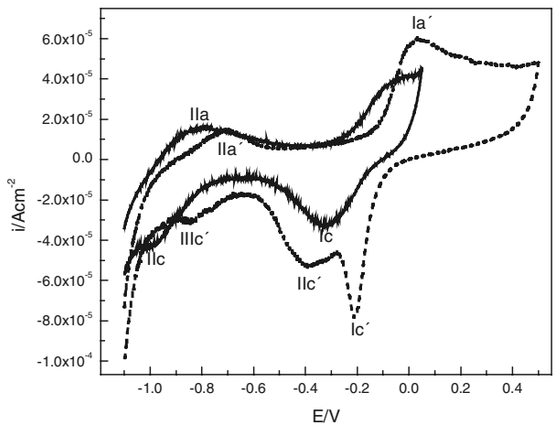


*Figure 4* Cyclic voltammogram of brass in deaerated artificial tap water (ATW) (—) and in borax buffer pH 7.8 (- - -). Scan rate: 10 mV $s^{-1}$.

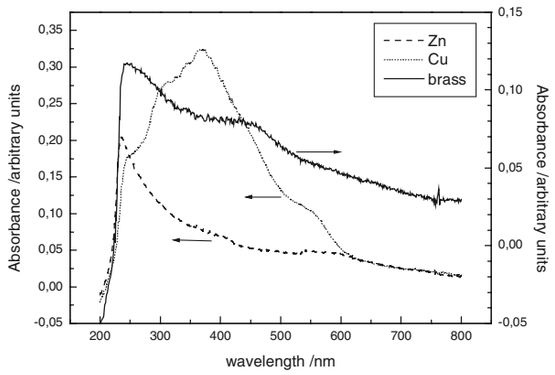


*Figure 5* Reflectance spectra typical of copper, brass and zinc electrodes held at open circuit potential (OCP) for 2 h.

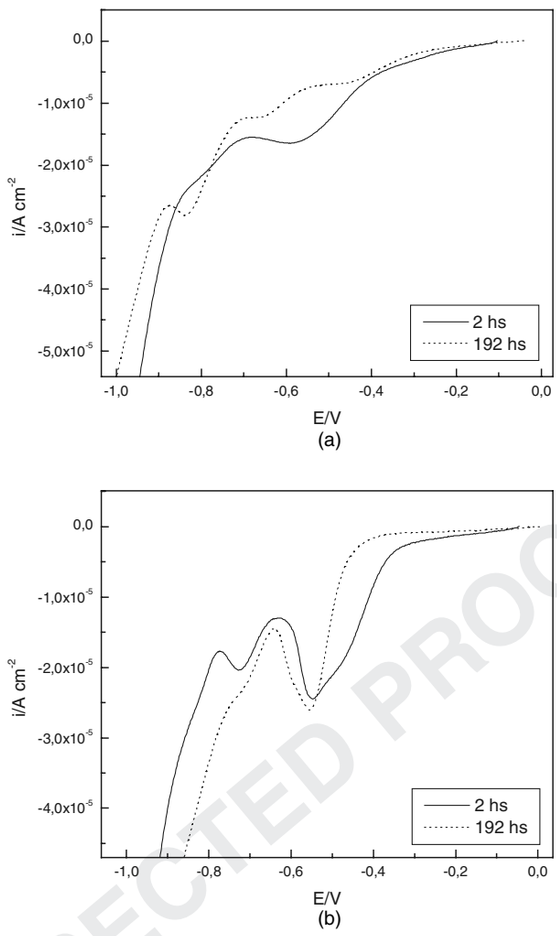


*Figure 6* Potentiodynamic reduction of the surface film grown on (a) copper and (b) brass after holding the electrodes for 2 and 192 h at open circuit potential (OCP). Scan rate: 1 mV $s^{-1}$.

The OCP stabilizes at around –0.017 V in the case of copper and −0.912 V in the case of zinc, while in the case of brass the OCP is –0.006 V (average of over 25 measurements).

Fig. 5 presents the reflectance spectra typical of copper, brass and zinc electrodes held at OCP for 2 h. In the case of copper, the absorbance peaks at 237, 314 and 380 nm together with shoulders at 462 and 550 nm are characteristic of $Cu_2O$ [25, 31]. Their presence points at cuprous oxide as the main component of the surface film. As for brass, the main peaks are again present but with different intensities. A peak at 462 nm suggests the presence of $Cu_2O$. There is also a peak at 260 nm, which corresponds to the main feature of the Zn surface spectrum. This can be ascribed to zinc oxo-hydroxides [32].

When the copper film that grows after two hours at OCP is potentiodynamically reduced, two cathodic peaks appear at −0.61 and −0.85 V (see Fig. 6a), in good agreement with those found in the voltammogram shown in Fig. 2. A new spectrum recorded after the reduction process shows no evidence of surface films. The reduction current for a film grown during 192 h at OCP is also presented for comparison.

In the case of brass, when the film is potentiodynamically reduced, two cathodic peaks appear at −0.65 and −0.88 V (Fig. 6b), again in good agreement with those in the cyclic voltammogram (Fig. 4). After 192 h, it can be observed that the intensity of the peak attributed to the reduction of Zn(II) species increases markedly when compared to the intensity of the $Cu_2O$ reduction. The total charge associated to the reduction processes decreases when the materials are aged for longer times (Fig. 6a and b).

Reflectance spectroscopy can also be used to evaluate the rate of growth. Reflectance spectra were recorded at 30, 60, 90 and 120 min. No differences could be found as regards the amount and the position of the peaks, when both materials are compared to the corresponding 24-h spectrum [9]. Fig. 7a and b present the semi-logarithmic relationship between absorbance and time for copper and brass respectively. The wavelength corresponds to the peak of maximum intensity for each spectrum. As can be seen, the absorbance follows a linear relation with log ($t$) for both materials. In addition, the slopes present similar values, being 0.0030 for copper and 0.0027 for brass (average of 5 independent measurements). This can be taken as an indication of the fact that the surface oxides on both materials grow at the same rate.

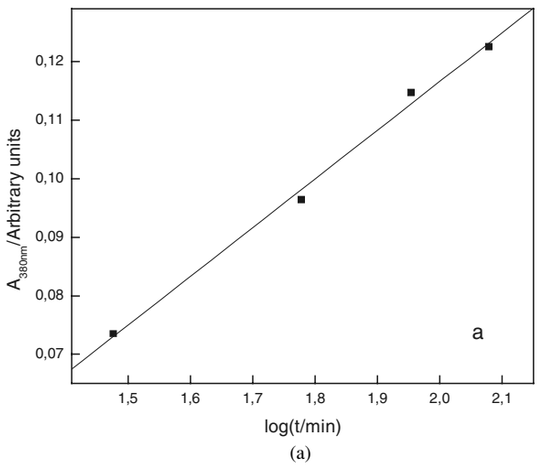


*Figure 7* Semi-logarithmic relationship between absorbance and time for (a) copper and (b) brass. $\lambda_{Cu} = 380$ nm and $\lambda_{brass} = 450$ nm.

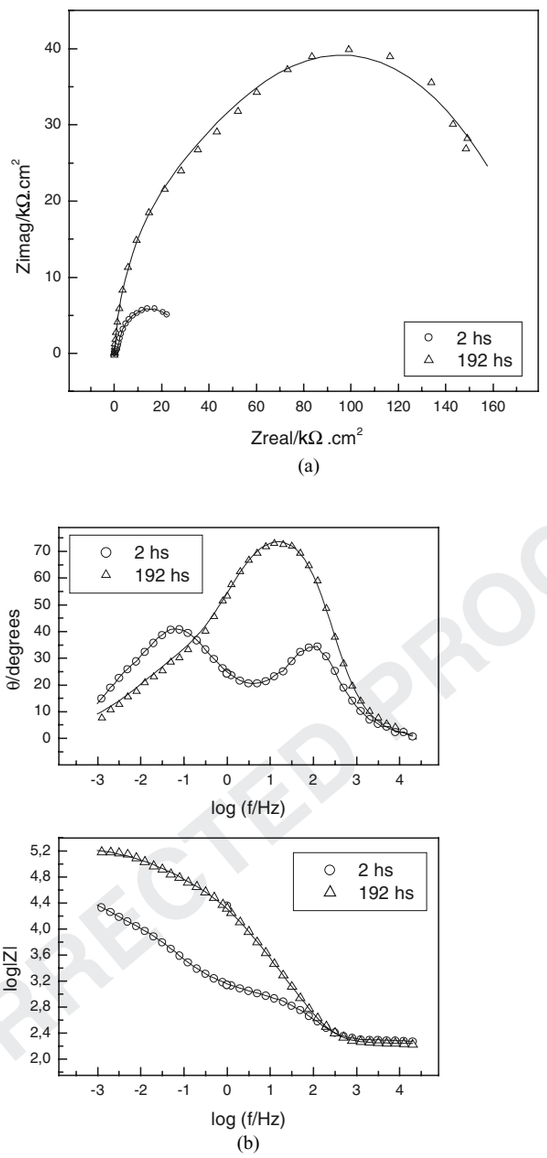


*Figure 8* Impedance spectra recorded on copper electrodes held for 2 and 192 h at OCP. The symbols represent the data and the lines the fitting results. During the fitting procedure, the equivalent circuit presented in Fig. 1 has been employed. (a) Nyquist representation; (b) Bode representation.

## 3.3. Characterization of the surface films formed at open circuit potential by electrochemical impedance spectroscopy

Impedance spectra were recorded in the form of Nyquist and Bode plots, on copper and brass electrodes held for 2 and 192 h at OCP. The results are shown in Figs 8 and 9 for copper and brass respectively. As can be seen, the impedance spectra present two time constants. An schematic representation of the structure of the surface film present on the metallic surfaces after ageing in ATW as well as the corresponding equivalent circuits are presented in Fig. 1. EIS data fit results are shown in Figs 8 and 9, together with the recorded data. $R_s$ represents the solution resistance, $Q_o$ a constant related to the surface oxide, $R_o$ the resistance to current flow through defects in the surface oxide, $Q_{dl}$ a constant related to the double layer and $R_{dl}$ the polarization resistance.

The experimental data were found to fit reasonably the proposed equivalent circuit. In the case of electrodes aged for 192 h, $n_{dl}$ was fixed at 0.5 during the fitting procedure to simulate a Warburg element. The optimised parameter values are presented in Table I. From the polarization resistance values, the corrosion current density was calculated using Equation 1. The results are shown in Table II.

## 3.4. Corrosion resistance of the surface films formed at open circuit potential

Anodic and cathodic polarization curves for copper and brass are presented in Fig. 10a and b, respectively. The results are shown superimposed for electrodes aged during 2 and 192 h. For each curve, the potential sweep started at the OCP and was then scanned either in the negative or in the positive direction, in independent experiments using two different electrodes. The corrosion current can be determined from the intercepts of the polarization curves (see Table II). Also, Tafel slopes can be evaluated from the linear portion of E vs. log

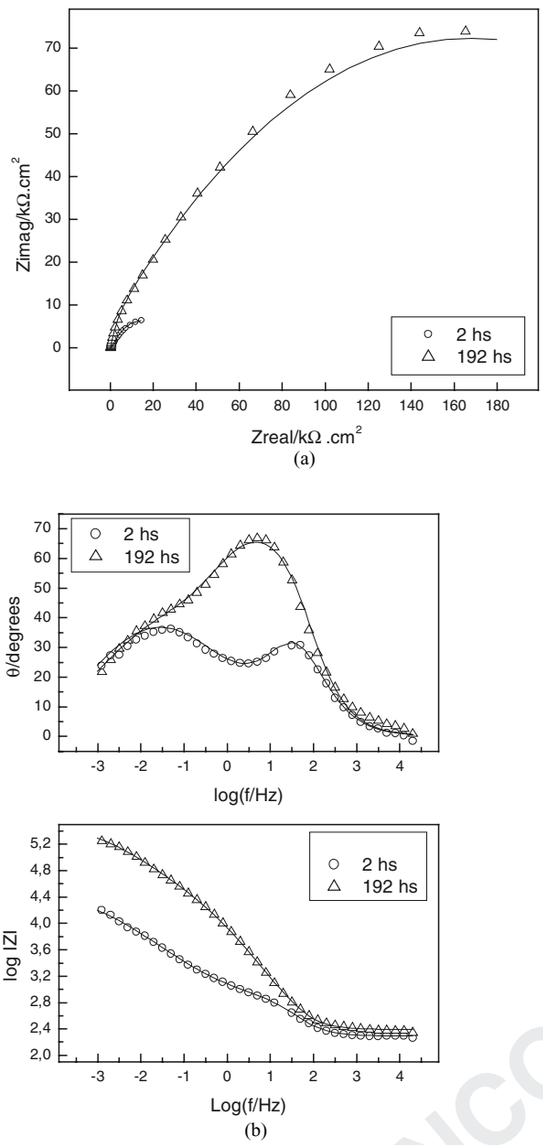


*Figure 9* Impedance spectra recorded on brass electrodes held for 2 and 192 h at OCP. The symbols represent the data and the lines the fitting results. During the fitting procedure, the equivalent circuit presented in Fig. 1 has been employed. (a) Nyquist representation; (b) Bode representation.

(i) curves. Tafel slopes, together with the value for the coefficient B in Equation 1 are summarized in Table III. The anodic Tafel slopes are in excellent agreement with those calculated by Feng *et al*. for copper at different immersion times in neutral tap water [13]. Thus, if a one electron exchange is assumed [33], the deviation from the theoretical 60 mV/decade can be attributed to imperfections in the film structure, such as porosity. In the case of copper, the calculated value for the parameter B (involving the cathodic Tafel slope, as well) is also in good agreement with the value 0.0245 V proposed by Feng and col. [13]. In the case of brass, experimental Tafel slope values have not been reported in the literature. Badawy and col. [15] assumed Tafel slopes of 0.12 V and $B = 0.026$ V for a lead-brass alloy in neutral solutions.

TABLE I Optimized values for the parameters employed in fitting the data in Fig. 8 using the equivalent circuit proposed in Fig. 1

| Element | Brass 2 hs | Copper 2 hs | Brass 192 hs | Copper 192 hs |
|---|---|---|---|---|
| $R_s/\Omega cm^2$ | 208 | 192 | 217 | 166 |
| $Q_o/\Omega^{-1}\ cm^{-2}S^N$ | $3.1\times10^{-5}$ | $1.2\times10^{-5}$ | $2.8\times10^{-5}$ | $6.6\times10^{-6}$ |
| $n_o$ | 0.81 | 0.85 | 0.87 | 0.86 |
| $R_o/\Omega cm^2$ | 767 | 809 | 33382 | 21858 |
| $Q_{dl}/\Omega^{-1}\ cm^{-2}\ S^N$ | $3.3\times10^{-4}$ | $5.6\times10^{-4}$ | $3.5\times10^{-5}$ | $4.88\times10^{-5}$ |
| $n_{dl}$ | 0.57 | 0.66 | 0.5 (fixed) | 0.5 (fixed) |
| $R_{dl}/\Omega cm^2$ | 29891 | 24739 | 339966 | 193347 |

TABLE II Corrosion current density values determined for copper and brass held for 2 and 192 h at OCP, using different techniques. $i_{corr\ EIS}$ is calculated after fitting EIS results with the equivalent circuit in Fig. 1. $i_{corr\ pol}$ is calculated from the interception of the polarization curves in Fig. 10. $i_{corr\ Rp}$ is calculated from the polarization resistance measurements using Equation 1

| | Time (h) | $i_{corrEIS}$ (A $cm^{-2}$) | $i_{corr\ pol}$ (A $cm^{-2}$) | $i_{corr\ Rp}$ (A $cm^{-2}$) |
|---|---|---|---|---|
| Copper | 2 | $8.1\times10^{-7}$ | $3.5\times10^{-7}$ | $8.6\times10^{-7}$ |
| | 192 | $1.4\times10^{-7}$ | $1.6\times10^{-7}$ | $1.9\times10^{-7}$ |
| Brass | 2 | $3.7\times10^{-7}$ | $2\times10^{-7}$ | $4.5\times10^{-7}$ |
| | 192 | $4.7\times10^{-8}$ | $5\times10^{-8}$ | $6.8\times10^{-8}$ |

TABLE III Tafel slopes evaluated as the slope of the linear portion of the E vs. log (i) curves shown in Fig. 10. Coefficient B is defined in Equation 1. $B = \frac{\beta_a\beta_c}{2.303(\beta_a+\beta_c)}$

| | | $\beta_c$/V | $\beta_a$/V | B/V |
|---|---|---|---|---|
| Copper | 2 hs | 0.104 | 0.079 | 0.020 |
| | 192 hs | 0.123 | 0.093 | 0.027 |
| Brass | 2 hs | 0.054 | 0.045 | 0.011 |
| | 192 hs | 0.064 | 0.086 | 0.016 |

The corrosion current can also be calculated from polarization resistance measurements carried out by potential sweeps in the vicinity of the OCP, as described in Section 2.3 for copper and brass electrodes held for 2 and 192 h at OCP in ATW. These values can be seen in Table II, where they are compared with corrosion current density values calculated employing various experimental techniques.

## 4. Discussion

This investigation aims at studying the composition and the protectiveness of surface oxide films naturally grown on copper and brass in contact with artificial tap water during 2 and 192 h.

By comparing the cyclic voltammograms of copper, zinc and brass in borax and in ATW, the different peaks could be assigned to Cu(I), Cu(II) and Zn(II) species. Taking into account the OCP potentials reported in Section 3.2., it can be suggested that the surface film is mainly composed by cuprous oxide. This can be confirmed by the results from the reflectance spectra registered for both materials, which were also described in Section 3.2. However, Zn(II) species are incorporated in the surface film grown on brass, as detected by the corresponding peak in the reflectance spectra (Fig. 5). The composition of the surface films grown at OCP

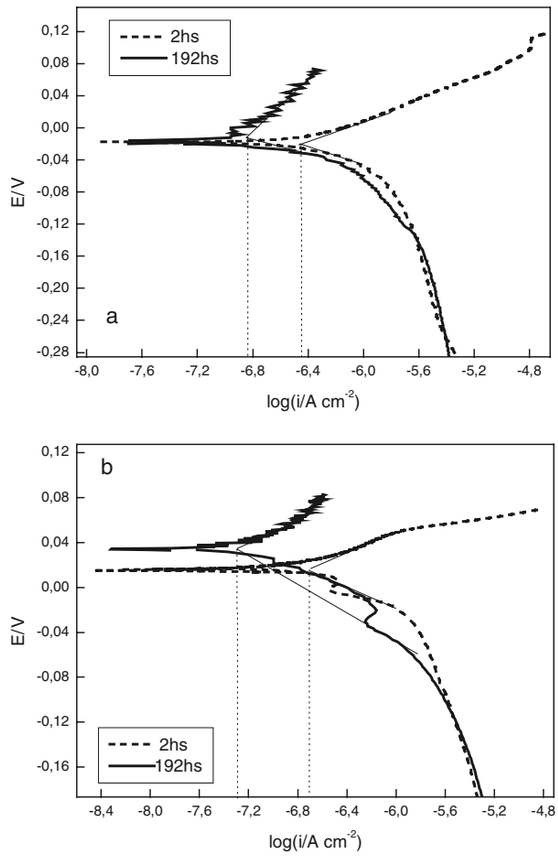


*Figure 10* Anodic and cathodic polarization curves for (a) copper and (b) brass. The curves were recorded after holding the electrodes 2 and 192 h at open circuit potential (OCP). Each curved started at OCP. Scan rate: 0.1 mV $s^{-1}$.

was finally confirmed by potentiodynamic reduction of the oxide layer.

On brass, the composition of the passive film is clearly influenced by the presence of Zn as alloying element, in agreement with previous findings in different electrolytes [14, 28]. When reflectance spectra are registered progressively in time, it was observed that only the intensity increases in time, indicating that merely the thickness is changing, without affecting the composition of the surface films. Also, from the slope of the curve in Fig. 7 it can be argued that the surface film on both materials grows at a similar rate.

When the oxides grown at fixed times and characterized by reflectance spectroscopy are potentiodynamically reduced, it can be seen that the resulting currents on brass are much lower than on copper (Fig. 6). This can suggest that the surface film that grows on brass is much more difficult to reduce than the one that grows on copper.

As regards EIS fitting results (Table I), it can be observed that all of the parameters calculated by fitting the experimental data with the equivalent circuit proposed in Fig. 1 present reasonable values. Furthermore, in the case of copper, the values are in excellent agreement with those presented by other authors for similar environments [1, 2].

A surface film can be considered stable and passivating if $Q_o$ shows little change in time, along with a corresponding increase in $R_{dl}$. This is the case for both materials, with the effect of time being slightly more evident for brass. At 192 h the results also suggest a better performance of brass, which is supported by field experience.

The oxide surface film is characterized by the parameter $n_o$. Values close to 0.9 are typical of porous films [23, 34]. As discussed above, the film on the substrates under study is mainly composed by $Cu_2O$, with the incorporation of Zn(II) species in the case of brass. The resistance associated to this layer ($R_o$) increases with time suggesting that the film becomes more compact [2]. Both the increase and the absolute value of $R_o$ are higher in the case of brass, which can be associated to the incorporation of Zn(II) oxo-hydroxides detected by reflectance spectroscopy.

Finally, for those surfaces aged during 192 h, the presence of a constant phase element where $n$ has been fixed to 0.5 in the fitting process, can be associated to the diffusion of a charged species through the surface layer. Diffusion processes in surface films on copper have been found before by other authors [3, 12, 34, 35].

Due to the low solubility of Cu(I) at neutral pH values, copper oxidation could be represented by:

$$Cu + OH^- \rightarrow Cu(OH)_{ad} + e \qquad (3)$$

The corrosion process on brass has been related before to non-steady state volume diffusion of zinc in the alloy [36 ].

The effect of ageing the electrodes for 192 h can also be appreciated in the polarization curves, particularly in the anodic one. There is almost no effect on the cathodic current, which can be attributed to oxygen reduction. Simultaneously, the anodic current is markedly reduced in the presence of a more compact and dense film. This densification process of the surface film apparently increases the resistance to diffusion imposed to charged species within the oxide layer (most likely Cu(I) species for copper and Cu(I) and Zn(II) species for brass). Diffusion of species associated to the cathodic hemi-reaction could be disregarded. This change in the structure of the film can also be related to the increase of the Tafel slopes with immersion time, which is stronger for the anodic branch (see Table III). Similar results for copper corrosion in tap water have been found before by other authors [12].

The corrosion current for both materials was calculated using various techniques: interception of the polarization curves and polarization resistance (which, in turn, can be evaluated from potential sweeps and from impedance spectroscopy). The results are compared in Table II. The values calculated form the different techniques are in reasonable agreement, both among themselves as in comparison with previously reported weight loss data for the same system [10] as well as with values from other authors [13]. As can be seen, the corrosion current density decreased in time, particularly in the case of brass. In this alloy, prolonged immersion improves the corrosion resistance, as found before by Ismail *et al.* in borate solution [16].

## 5. Conclusions

The composition of the surface film that grows at open circuit potential on copper and brass in artificial tap water was analyzed using *in-situ* techniques. The experimental system simulates a situation of practical interest, taking into account that brass is frequently chosen to build potable water distribution systems.

The electrical and spectrochemical features revealed that the oxide layer is mainly composed by cuprous oxide and that Zn(II) compounds incorporate into the brass film structure. As demonstrated by reduction curves and reflectance spectroscopy, the composition of the film is not influenced by the ageing time. Furthermore, the film grows at the same rate on both materials.

The film grown for 192 h becomes more compact and dense. It presents higher Tafel slopes and lower charge when potentiodynamically reduced.

Lower corrosion currents and lower anodic currents in the polarization curves are evident for brass after 192 h in contact with ATW. This improvement in the performance of the film on brass can be attributed to the larger incorporation of Zn(II) species into the surface layer, particularly as the film consolidates at longer times.

## Acknowledgements

This work has been supported by the National Research Council of Argentina, CONICET, (Project PIP 02570) and by the Universidad Nacional de Mar del Plata (Project 15/G115). M. B. Valcarce wishes to thank CONICET, Argentina, for her fellowship.

## References

1. A. PALIT and S. PEHKONEN, *Corros. Sci.* **42** (2000) 1801.
2. J. SHIM and J. KIM, *Mater. Let.* **58** (2004) 2002.
3. K. SOBUE, A. SUGUHARA, T. NAKATA, H. IMAI and S. MAGAINO, *Surf. Coat. Tech.* **169–170** (2003) 662.
4. A. E. BROO, B. BERGHULT and T. HEDBERG, *Corros. Sci.* **39**(6) (1997) 1119.
5. L. P. COSTAS, *Mater. Perform.* **9** (1977) 16.
6. P. BREMER and G. GEESEY, *Appl. Envir. Microbiol.* **57**(7) (1991) 1956.
7. B. J. WEBSTER, S. E. WERNER, D. B. WEELS and P. J. BREMER, *Corrosion* **56**(9) (2000) 942.
8. D. WAGNER and A. H. L. CHAMBERLAIN, *Biodegradation* **8** (1997) 177.
9. M. B. VALCARCE, J. P. BUSALMEN and S. R. D. SÁNCHEZ, *Int. Biodet. and Biodegr.* **50** (2002) 61.
10. M. B. VALCARCE, S. R. D. SÁNCHEZ and M. VÁZQUEZ, *Corros. Sci.* **47** (2005) 795.
11. J. P. BUSALMEN, M. B. VALCARCE and S. R. D. SÁNCHEZ, *Corros. Rev.* **22** (2004) 277.
12. Y. FENG, W. K. TEO, K. S. SIOW, K. L. TAN and A. K. HSIEH, *Corros. Sci.* **38** (1996) 369.
13. Y. FENG, W. K. TEO, K. S. SIOW and A. K. HSIEH, *ibid.* **38** (1996) 387.
14. W. A. BADAWY and F. M. AL-KHARAFI, *Corrosion* **55**(3) (1999) 268.
15. W. A. BADAWY, S. S. EL-EGAMY and A. S. AZAB, *ibid.* **53**(11) (1997) 842.
16. K. M. ISMAIL, S. EL-EGAMY and M. ABDELFATAH, *J. Appl. Electrochem* **31** (2001) 663.
17. K. M. ISMAIL, R. M. ELSHERIF and W. A. BADAWY, *Electrochimica Acta* **49**(28) (2004) 5151.
18. L. M. ABRANTES, L. M. CASTILLO, C. NORMAN and L. M. PETER, *J. Electroanal. Chem.* **163** (1984) 209.
19. H. H. STREHBLOW and B. TITZE, *Electrochim. Acta* **25** (1980) 839.
20. R. BABIK, M. METIKOS-HUKOVIC and A. JUKIC, *J. Electrochem. Soc.* **148**(4) (2001) B146.
21. H. H. STREHBLOW and H. D. SPECKMANN, *Werks und Korros.* **35** (1984) 512.
22. M. STERN and A. L. GEARY, *J. Electrochem. Soc.* **104** (1957) 56.
23. I. SCRIBNER ASSOCIATES, *ZPlot for Windows.* 1998.
24. L. J. ALJINOVIC, S. GUDIC and M. SMITH, *J. Appl. Electrochem* **30** (2000) 973.
25. S. R. D. SÁNCHEZ, L. E. A. BERLOUIS and D. J. SCHIFFRIN **307** (1991) 73.
26. S. CERÉ and M. VÁZQUEZ, *J. Mater. Sci. Lett.* **21**(6) (2002) 493.
27. R. M. SOUTO, S. GONZALEZ, R. C. SALVAREZZA and A. J. ARVIA, *Electrochim. Acta* **39**(17) (1994) 2619.
28. I. MILOSEV and H. H. STREHBLOW, *J. Electrochem. Soc.* **150**(11) (2003) B517.
29. J. MORALES, G. T. FERNANDEZ, P. ESPARZA, S. GONZALEZ, R. C. SALVAREZZA and A. J. ARVIA, *Corros. Sci.* **37**(2) (1995) 211.
30. M. POURBAIX, *Atlas of Electrochemical Equilibria in Aqueous Solutions* (Brussels: Pergamonn Press, Cebelcor, 1974).
31. R. E. HUMMEL, *Phys. State Sol. (a)* **76**(11) (1983) 12.
32. B. S. KIM, S. N. PIAO, S. N. HOIER and S. M. PARK, *Corros. Sci.* **37**(4) (1995) 557.
33. D. J. SCHIFFRIN and S. R. SÁNCHEZ, *Corrosion* **41**(1) (1985) 31.
34. M. E. FOLQUER, S. B. RIBOTTA, S. G. REAL and L. M. GASSA, *ibid.* **58**(3) (2002) 240.
35. M. METIKOS-HUKOVIC, R. BABIC and I. PAIC, *J. Appl. Electrochem* **30** (2000) 617.
36. A. P. PCHELNIKOV, A. D. SITNIKOV, T. K. MARSHAKOV and V. V. LOSEV, *Electrochim. Acta* **26** (1981) 591.

*Received 29 December 2004*
*and accepted 13 June 2005*